Pansharpening of Panchromatic Aerial Photographs by Combining Component Substitution and Multiresolution Analysis Fusion Algorithms

Salah, M.
Department of Surveying Engineering, Shoubra Faculty of Engineering, Benha University, Cairo, 11269 Egypt, E-mail: engmod2000@yahoo.com

Abstract
The monochromatic nature of aerial photographs may affect the accuracy of photogrammetric measurements. In this study, multispectral (MS) IKONOS images with 3.2 m spatial resolution are used to sharpen panchromatic (PAN) archival aerial photographs. An urban area with a variety of land use/cover (LULC) classes over the northeast region of Cairo city, Egypt has been selected. The proposed approach can be performed through two major steps. First and after pre-processing, Gram-Schmidt transform (GST) and wavelet fusion techniques were used to panshrpen the original MS bands. Second, a fuzzy majority voting (FMV) - based approach was designed to combine the results from the GST and wavelet techniques to predict the final high-resolution results. The results were visually, qualitatively, and quantitatively analyzed. Compared with GST and wavelet standard fusion techniques, the improved statistical indices, as well as the improved classification potential, confirmed the credibility of the proposed approach.

1. Introduction and Literature Review

Archival aerial photographs are essential for updating the register of buildings and lands. These photographs present valuable details of land use/cover (LULC) (Siok and Ewiak, 2020). On the other hand, it is difficult to collect satellite images with the same high-resolution as aerial photographs because of sensor design limitations (Qu et al., 2018). In Egypt, over 90% of cadastral maps have been generated and/or updated based on aerial photographs. Unfortunately, the interpretation of such aerial photographs is a challenge because of their monochromatic nature which may affect the accuracy of the feature extraction process, as well as the photogrammetric measurements.

Simulation of color aerial photographs with the same pixel size as the monochromatic ones allows a more accurate interpretation of objects. Pansharpening is a technique that combines high-resolution (HR) panchromatic imagery (PAN) with low-resolution (LR) multispectral (MS) ones to generate a new high spatial resolution/multispectral imagery (Klonus, 2008). If imagery from the same sensor are used for pansharpening, the ratio of ground sampling distances (GSD) between the panchromatic and the multispectral imagery is referred to as resolution ratio (RR). This ratio may range from 1:2 to 1:5. For imagery from different sensors, the RR can get larger. Pansharpened imagery have proved better performance in urban development and mapping (Pohl, 2016), LULC classification (He et al., 2018), feature detection (Matteoli et al., 2018), land monitoring (Murray et al., 2018), change detection (Liu et al., 2018), and decision-making process (Siok et al., 2020).

A variety of pansharpening algorithms were introduced and can be classified into four classes: Component substitution (CS); multi-resolution analysis (MRA); hybrid methods (HM); and learning-based algorithms (LBA). Typical examples of CS approaches are Intensity/hue/saturation transform (IHS) (Carper et al., 1990), Gram–Schmidt transforms (GST) (Aiazzi et al., 2007), Brovey transform (BT) (Maglione et al., 2016) and Principle component analysis (PCA) (Shahdoosti and Ghassemian, 2016). These algorithms usually perform well in terms of processing time, preserving the spatial details of the PAN image and robustness to mismatches between the panchromatic and multispectral bands. However, these approaches usually result in spectral distortion (Duran et al., 2017). The main limitation of the IHS and BT approaches is that the input data should not exceed three multispectral bands (Pouran, 2005). The MRA approaches include the Laplacian pyramid (LP) (Burt and Adelson, 1983), Contourlets (Do and Vetterli, 2005), wavelet transform (WT) (Zhang et al., 2009).

This category has proved to be efficient in preserving the spectral details, while it is very sensitive to misalignments between the panchromatic and multispectral bands (Xu et al., 2014). This conforms to results obtained by Mhangara et al., (2020). The hybrid approaches take advantages of both the CS and MRA techniques and therefore have the ability of preserving the spatial/spectral information. This category includes algorithms such as non-separable wavelet frame transform (NWFT) (Li et al., 2005) and Guided filters in PCA domains (GFs/PCA) (Liao et al., 2015).

Many studies have been undertaken to solve for the limitations of single pansharpening algorithms by effectively combining two or more fusion approaches. Ehlers et al., (2010) integrated IHS and fast Fourier transforms (FFT) algorithms for multi-sensor/multi-temporal image fusion. However, the high-pass and low-pass filters for PAN and MS images make the process complex. Johnson et al., (2013) integrated IHS with smoothed filter intensity modulation-based approach (SFIM) for image pansharpening. The results showed that as the spatial ratios of MS/PAN images decrease, the quality of the obtained images decrease. Zhong et al., (2017) combined MRA-based and CS approaches. Though the obtained images are spectrally higher, the proposed approach fails to preserve the spatial properties. Faragallah (2018) fused PAN and MS images by combining high-pass modulation (HPM) with adaptive PCA (APCA). The proposed approach has proved to work well for single-sensor images. For multi-sensor image fusion, as the spatial ratios of MS/PAN images decrease, the quality of the obtained images decrease. Zhang et al., (2019) fused PAN and MS images using spatially weighted neighbor embedding (SWNE). The proposed approach resulted in a spatially high-fused image with lower spectral quality.

Recently, deep learning (DL)-based image pansharpening has become an active topic of research. The LBA category aims at learning the mathematical relationship between the PAN, MS, and the pansharpened imagery (Azarang and Ghassemian, 2017, Hu et al., 2019 amd Xu et al., 2020). However, the application of such algorithms depends heavily on learning abilities and requires many prior assumptions. As well, several difficulties can also be experienced during implementation such as mismatches between the PAN and MS imagery may have a devastating impact on the obtained results (Krizhevsky et al., 2012); and low-quality training samples can seriously deteriorate the pan-sharpened image (Shocher et al., 2018).

Several studies have been performed to investigate the potential of pansharpening of panchromatic images. These include imagery from IKONOS-2 and WorldView-2 (Vivone et al., 2015); Sentinel-2 (Vaiopoulos and Karantzalos, 2016); GÖKTÜRK-2 (Kahraman and Ertürk, 2017); UAV images (Jenerowicz et al., 2018a); radar imagery (Jenerowicz et al., 2018b); SPOT-6 (Mhangara et al., 2020); and GeoEye-1, QuickBird, KompSat-2, KompSat-3A, TripleSat, Pleiades-1, and Deimos-2 (Javan et al., 2021). Compared to studies conducted on satellite imagery, quite a few studies are available concerning the fusion of PAN aerial images and MS satellite data (Ewiak et al., 2016, Siok et al., 2017 and Ewiak et al., 2018). Siok et al., (2020) proposed an approach for combining PAN aerial imagery and Sentinel-2 MS satellite imagery. The pansharpened images showed less spectral distortion compared with traditional approaches of image pansharpening. Kaimaris et al., (2020) reported a significant increase in the interpretation ability from archival PAN aerial photographs as a result of combining them with archival MS satellite imagery.

A detailed review of image pansharpening techniques can be found in Wang et al., (2005), Kahramana and Ertürk (2017), Mhangara et al., (2020) and Javan et al., (2021). In conclusion, for imagery acquired by one sensor at the same time (single-sensor/single-date), most of the pansharpening algorithms provide accurate results. These algorithms can still generate spatially enhanced imagery for multi-sensor/multi-date pansharpening, but usually with a negative impact upon the spectral consistency (Ehlers et al., 2010).

All of the above approaches have their advantages and disadvantages; however, still there is unlimited room to enhance the spatial/spectral qualities of the panshrpened images. To solve such a pansharpening problem, this study proposes a new hybrid model for pansharpening of PAN aerial photographs with archival MS satellite imagery. In this regard, the results obtained for two pansharpening algorithms have been combined based on fuzzy majority voting (FMV). These algorithms are wavelet fusion (wavelet) and Gram–Schmidt transforms (GST). Since the GST algorithm results in high spatial quality while the wavelet results in high spectral quality, the optimal fusion of such algorithms can result in minimum spectral/spatial distortions.

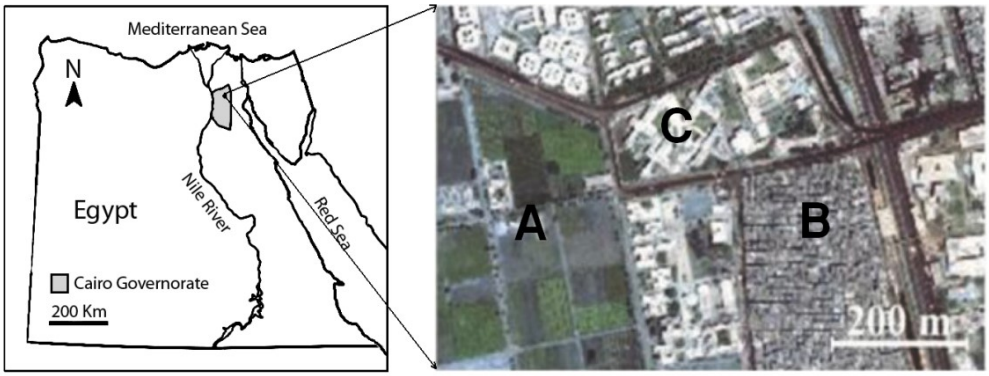

Figure 1: The geographical location of the test area (left); the test area (right). A denotes vegetation and agricultural fields, B refers to roads and high-density built-up areas, and C stands for urban areas

Table 1: datasets used for experiments

GSD (m)	*Acquisition Date*	*Sensor*
0.15	July 22, 2017	Film Camera
3.2	April 17, 2010	IKONOS

(a) (b) (c)

Figure 2: The datasets used in the experiments: (a) MS IKONOS image; (b) PAN aerial image; (c) DEM

2. Study Area and Data Sources

The study area used in this research covers an urban area over Cairo city, Egypt. Figure 1 (left) shows the geographical location of test area. A subset of 750 × 850 m has been applied for the experiments as shown in Figure 1 (right). The landscape is varied including vegetation and agricultural fields on the left, roads and high-density built-up areas on the right and urban areas with different roof types such as concrete and metal at the middle and upper parts. This will help to investigate the spectral and spatial consistency of the pansharpened images.

The selection of datasets for the experiments was aimed at the collection of images with no LULC changes and zero percentage cloud cover. In this regard, a PAN aerial image acquired by the Egyptian Survey Authority (ESA) on July 22, 2017, has been fused with IKONOS image at 3.2 m GSD. The IKONOS image was acquired on April 17, 2010, with RGB (red, green, and blue) spectral bands as shown in Figure 2a. On the other hand, the film camera aerial photographs were collected at a scale of 1:10,000. The film was scanned in one PAN band with 15µm (GSD = 0.15 m) as shown in Figure 2b. Although the difference of acquisition dates between the two datasets exceeds seven years, no serious changes related to natural disasters, human activities, or illumination conditions can be observed in the study area. This will keep the spectral distortion of the obtained images to a minimum. Table 1 summarises the characteristics of the used datasets.

Both PAN aerial photographs and MS satellite imagery have been orthorectified and spatially registered in the UTM/WGS84-zone 36 projection. In this regard, the nearest neighbor resampling technique has been applied to resample all bands of the MS IKONOS image (3.2 m) to the GSD of the PAN aerial one (0.15 m). For orthorectification of aerial and satellite imagery, 12 control points (CPs) along with a digital elevation model (DEM) obtained from a stereo pair of the same aerial photographs with GSD of 1 m have been used as shown in Figure 2c. The ellipsoidal heights range from 9 to 231 m with dark colors refer to lower elevations while light colors refer to higher ones.

3. Methodology

This section introduces the proposed approach in detail. After the postprocessing stage, the GST and wavelet algorithms have been applied to generate two different pansharpened images. The FMV was then adopted to combine the GST and wavelet results. Finally, the visual, spatial, and spectral properties of the FMV fusion results have been evaluated (Figure 3).

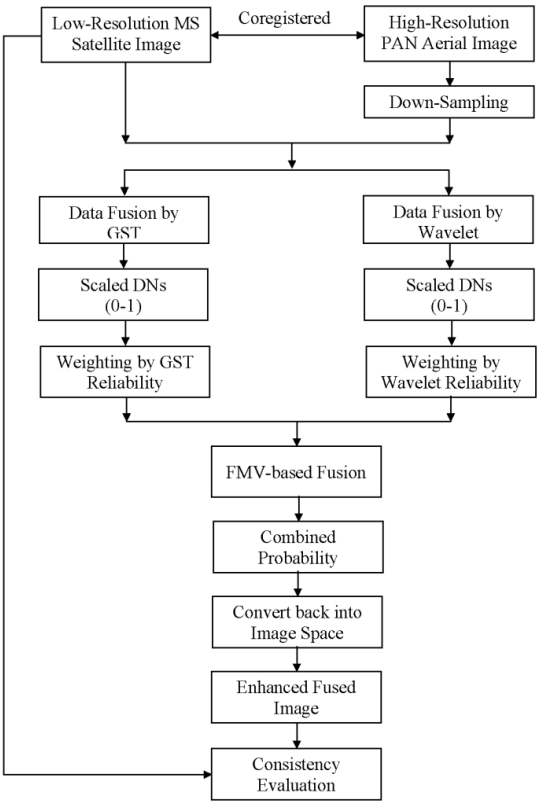

Figure 3: Flowchart of the hybrid FMV fusion

3.1 Image Fusion Algorithms

In the first stage, the PAN aerial photograph band and the MS satellite image have been applied as input data for two standard fusion techniques which are the GST and the wavelet algorithms.

3.1.1 Gram–Schmidt Transform (GST)

Recently, GST has become one of the most commonly used pansharpening techniques. It is a standard algorithm in most commercial remote sensing packages such as ERDAS, ENVI, IDRISI, and PCI. A lower resolution PAN image ($\boldsymbol{L_P}$) is first simulated by averaging the MS bands at the same scale of the PAN image. After that, the $\boldsymbol{L_P}$ image along with the MS bands (upscale to the same scale as the PAN image) are applied as input for the GST with $\boldsymbol{L_P}$ image ranked as the first band. Then, the statistics of the PAN image are adjusted to match those of the first transform band (GST_{1LR}) that obtained from the GST to produce a modified PAN image. The GST_{1LR} is replaced with the modified PAN image to produce a new set of transform bands. Finally, an inverse GST is performed on the obtained new set of bands to produce the high resolution pansharpened MS images. The GST approach usually results in spectral distortions. Spatial details are obtained by subtracting the simulated PAN band from the original PAN one. To generate the pansharpened image, extracted spatial details are injected into the MS bands which are then resampled to the resolution of the original PAN band. The injection gain factor in the GST approach, g_k, can be defined using Equation 1 with *cov (.)* and *var (.)* are the covariance matrix and the variance value respectively (Laben et al., 2000). The mathematical model behind the GST is explained in several references (O'Connell, 1974, Gong et al., 2001 and Li et al., 2016).

$$g_k = \frac{\mathrm{cov}(\widetilde{MS}_k, I_L)}{\mathrm{var}(I_L)} \qquad K = 1, \ldots, N \qquad \text{Equation 1}$$

3.1.2 Wavelet

More recently, the wavelet fusion algorithm has proved to be effective for reducing the spectral distortion problem. Wavelets are mathematical models that cut up input data into different frequency components and then analyze each component with a different resolution according to its scale (Lemeshewsky, 2002). It is a multi-resolution decomposition in which the original image is substituted by a set of approximated bands LL_j and three detailed bands HL_j, LH_j, HH_j of low-resolution (resampled by 2) at different levels of decomposition j. The detailed bands (*HL; LH; HH*) represent the high-frequency features, while the approximated bands (*LL*) represent the low-frequency features, intensity. First, the MS image is transformed to the IHS space, and wavelet decomposition is performed on the I channel. The wavelet decomposition is then generated for the obtained decompositions. The detailed images HL_i; LH_i; HH_i; $\forall i \in [1; j]$ are collected from the PAN band's decomposition while the last LL^1 of MS image's decomposition is used to collect the *LL* image. Before the wavelet decomposition, the intensity ranges of both the PAN image and MS image (I channel) are matched (Coltuc et al., 2006). The final pansharpened image is then produced by recomposing the pansharpened decomposition as shown in Figure 4.

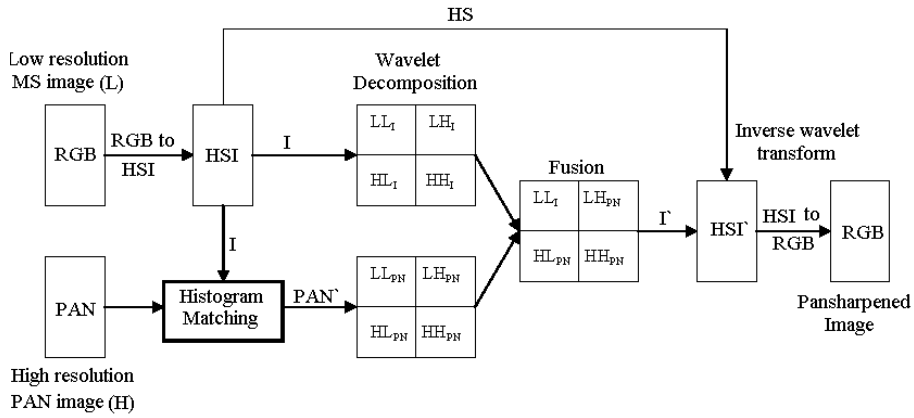

Figure 4: Flowchart of wavelet-based pansharpening

The major problem associated with the wavelet algorithm is the computational complexity compared with the standard approaches (Jiang et al., 2013). The mathematical model behind the wavelets is explained in several references (Zhang, 2002 and Wang et al., 2005).

3.1.3 FMV

In the second stage, the outputs from the GST and wavelet methods have been fused using the FMV algorithm to obtain an enhanced pansharpened image. Before applying the results obtained for the GST and the wavelet algorithms as input to the FMV algorithm, these images were linearly scaled (from zero to one) using Equation 2:

$$SDN = [(DN - DN_{Min}) / (DN_{Max} - DN_{Min})]$$

Equation 2

Where:

SDN: the scaled digital number of the pixel under investigation.

DN_{Min}: The minimum digital number.

DN_{Max}: The maximum digital number.

FMV is an efficient technique to handle the uncertainties in digital imagery. It applies a membership function to map a certain pixel (in the input space) as a membership value (in the output space). Before incorporating the *SDN* obtained for the GST and the wavelet algorithms into the FMV, the *SDN* is first weighted by the spatial and spectral consistency estimated for the GST and wavelet pansharpened images. Let the spatial and spectral consistencies obtained from the assessment process are *HCC* and *CC* respectively. The weighted scaled digital numbers *SDN*` can be expressed as follows:

$$SDN` = SDN * HCC * CC$$

Equation 3

Based on the weighted *SDN*, the membership function of relative quantifiers is then estimated for the GST and Wavelet pansharpened images as described in Equation 4, with typical *a* and *b* value range [0, 1]. For a given pixel, $Q_P = 0$ indicates that the quantifier has not fulfilled at all, while $Q_P = 1$ indicates that the quantifier has completely satisfied (Herrera and Verdegay, 1996).

$$QP = \begin{cases} 0 & if\ SDN` < a \\ \dfrac{SDN` - a}{b - a} & if\ a \le SDN` \le b \\ 1 & if\ SDN` > b \end{cases}$$

Equation 4

The optimal setting of the parameters (*a*, *b*) has a positive impact on the FMV-based fusion. These two parameters control the position and shape of the membership function Q_P. Up to now, no mathematical model is available to estimate such parameters (Saheb et al., 2013). To estimates the optimal *a* and *b* values, a grid-search with 10-fold cross-validation has been used. In this regard, a 0.1-grid interval has been applied to search for the optimal *a* and *b* simultaneously. As soon as the optima *a* and *b* values are reached, the membership function Q_P is estimated, and the weights based on the linguistic quantifier (*w*) are determined according to Equation 5 with *i* is the order of the GST and wavelet fusion algorithms after ranking Q_P in descending order and *N*=2, the total number of the applied fusion algorithms. As the last step, the fused digital number (DN_{fused}) based on FMV can be estimated as in Equation 6 (Yager, 1998).

In this regard, the original *DN* obtained for the GST and wavelet pansharpened images are

weighted by the corresponding linguistic quantifier The process is repeated with successive band selection until all bands from GST and wavelet results are combined.

$$w = QP`\left(\frac{i}{N}\right) - QP`\left(\frac{i-1}{N}\right), for\, i = 1\ ,\ .....\ , N$$

Equation 5

$$DN_{fused} = \arg\max_{N}\left[\sum_{i=1}^{N} w_i\ DN_i / 2\right]$$

Equation 6

Where:

w_i: the weights obtained for GST and wavelet algorithms.

DN_i: the digital number of the fused images by GST and wavelet algorithms.

For clarity, Table 2 is a typical example that shows the real calculations for one pixel using the proposed approach. The FMV-based fusion model has been implemented by the author in the Matlab 2017a environment under Windows 10 and CPU@3.20 GHz/16 GB RAM.

3.2 Evaluation Methods

The objective is to evaluate the ability of the proposed approach to improve spatial resolution while preserving the spectral characteristics. weight *w* and averaged according to Equation 6. Additionally, the execution time has been displayed for each fusion method. The descriptions of all statistical indices applied for evaluation are presented in Table 3.

3.2.1 Spatial evaluation

To evaluate the degree of spatial improvement, the high-pass correlation coefficient (*HCC*) was adopted. First, the PAN image and all bands of the pansharpened image have been filtered using a high-pass filter with 3x3-Laplacian kernel. The correlation coefficients (*CC*) between the high-pass filtered PAN and MS bands were then calculated. According to Pradhan et al., (2006), any HP filter can be applied for the evaluation process.

3.2.2 Spectral evaluation

Since the high-resolution MS reference data is not practically available, the original MS satellite image has been adopted as the reference data. In this regard, the pansharpened image has been downsampled to its original lower resolution and then compared with the original MS bands (Hu et al., 2019). The nearest neighbor resampling has been applied for downsampling to ensure a minimum change of the DN values (Mhangara et al., 2020).

Table 2: Fused *DN* estimation based on FMV

DN		***SDN***		***SDN'***		***Q_p***		***Q_p`***		***w***		DN_{fused}
GST	*WAV*	*GST*	*WAV*	*GST*	*WAV*	Q_{GST}	Q_{WAV}	$Q`_{GST}$	$Q`_{WAV}$	$w_{pp}`_{GST}$	$w_{pp}`_{WAV}$	
71	79	0.34	0.31	0.12	0.10	0.24	0.2	0.24	0.2	0.12	0.10	68

Table 3: Statistical indices applied for performance evaluation

	Index	***Description***	***Reference***
Spatial	*HCC*	The correlation between the original PAN image and the pansharpened bands after high-pass filtering. Higher values indicate better performance.	Zhou et al., (1998)
Spectral	*CC*	The correlation between the fused and the original MS bands. *CC* ranges from -1 to 1 with higher values indicate better performance.	Wang et al., (2004)
	RMSE	*RMSE* represents the quantitative similarity between the pansharpened and the original MS imagery. Smaller values indicate better performance.	
	DIV	The mean difference in variances between the fused and the original MS bands. Smaller values indicate better performance.	
	SSIM	The SSIM reveals the structural similarity. a larger value indicates better performance	
	UIQI	*UIQI* estimates the spectral differences between the pansharpened the original MS bands. Larger values indicate better performance.	
Classification	*OA*	The percent of reference data being correctly classified.	Congalton (1991)
	PA	The probability that reference samples being correctly detected.	
	UA	The probability that detected samples match the reference data.	

After that, five statistical indices have been applied to evaluate spectral preservation. These indices include: correlation coefficient (*CC*); root mean square error (*RMSE*); universal image quality index (*UIQI*); the difference in variance (*DIV*); and structure similarity (*SSIM*). The Matlab codes for these indices are available at http://openremotesensing.net/.

3.2.3 Classification accuracy

In a second investigation, the pansharpened images using the GST, wavelet, and hybrid approaches have been used, separately, as inputs for the maximum likelihood classifier. To estimate the classification accuracies, almost 150 randomly distributed points have been selected based on the original MS IKONOS image and used as reference data. Since the overall classification accuracy (*OA*) is a global measure for classification accuracy, the users and producers accuracies (*UA* and *PA*) have also been adopted. Unlike the *OA*, the *UA* and *PA* indicate how the pansharpened images improve or deteriorate the detection accuracy for individual classes.

4. Results and Analysis

To illustrate the research findings, Figure 5a and b show the PAN and MS images respectively. The fused image using the proposed FMV approach is an enhanced 3-band image with a GSD of 0.15 m as shown in Figure 5c.

4.1 Visual Analysis

To assess the performance of the proposed hybrid method for pansharpening of the PAN aerial images with the MS IKONOS imagery, three fused images have been generated for the GST, wavelet and the proposed hybrid approaches as shown in Figure 6a, b, and c respectively. It can be observed that the worst results have been obtained for the GST fusion as shown in Figure 6a. In this regard, color distortions are visible and the fused image is almost blurry. In some parts of the fused image, colors seem to be black and white (BW). A possible reason for such an observation is that the high spectral values in the PAN image have been replaced with low ones in the pansharpened image. The fused wavelet image shows better color preservation than the GST approach as shown in Figure 6b but not as the enhancement obtained for the hybrid approach. In terms of spectral and spatial characteristics, the best result has been obtained for the hybrid pansharpening approach. Compared to the original image, no distinct color changes can be observed while the spatial improvement is visible as shown in Figure 6c.

Figure 5: Results of applying the proposed pansharpening approach: (a) PAN aerial image; (b) MS IKONOS image; (c) the pan-sharpened image by the proposed approach

Figure 6: Fused images using: (a) GST; (b) wavelet; (c) hybrid approach

Table 4: Spatial evaluation of the results. Bold values indicate the best and underlined values indicate the worst

Method	**GST**	**Wavelet**	**Hybrid**
HCC	0.872	0.412	**0.956**

Table 5: Spectral evaluation of the results. Bold values indicate the best and underlined ones indicate the worst

Method	*HCC*	*CC*	*UIQI*	*RMSE*	*DIV*	*SSIM*	*CPU Time*
GST	0.872	0.400	0.88	5.512	45.33	0.389	**0.86 Sec/Km^2**
Wavelet	0.412	0.780	0.94	3.68	6.89	0.791	1.22 Sec/Km^2
Hybrid	**0.956**	**0.967**	**0.96**	**1.51**	**1.68**	**0.956**	1.31 Sec/Km^2

4.2 Spatial Evaluation

For spatial evaluation, the statistical measures presented in Table 3 have been estimated and evaluated. The spatial quality of the fusion algorithms has also been assessed. The results are presented in Table 4 with the most accurate values marked in bold and the worst are underlined. For the proposed hybrid approach, the spatial enhancement has proved to be sufficient. In terms of *HCC*, the GST and hybrid approaches are very consistent with average *HCC* values above 0.8. This high *HCC* value indicates that the fused image has maintained almost the detailed spatial information as the original PAN aerial image. The wavelet approach showed lower *HCC* than the GST and hybrid approaches, with *HCC* around 0.4. This low value indicates that there is no strong correlation between the pansharpened and the original high-resolution bands.

4.3 Spectral Evaluation

In terms of spectral enhancement, the hybrid approach resulted in the best performance as indicated by the *CC*, *UIQI*, *RMSE*, *DIV*, and *SSIM* values as shown in Table 5. The hybrid pansharpening approach had the highest *CC*, *UIQI*, and *SSIM* values of 0.967, 0.96, and 0.956 respectively. The best performance of the hybrid approach is further confirmed by the lowest *RMSE* and *DIV* values of 1.51 and 1.68 respectively. Again, the statistics indicate that the pansharpened image by the hybrid approach has maintained almost the spectral information as the input MS image. For instance, the *CC*, *UIQI*, *RMSE*, *DIV*, and *SSIM* of the proposed hybrid approach are 0.187, 0.02, 2.17, 5.21, and 0.165 better than the second-best fusion algorithm respectively. This demonstrates the high spectral resolution of the results obtained for the proposed pansharpening approach. The wavelet fusion algorithm ranked second in terms of retaining spectral information with *CC*, *RMSE*, and *SSIM* of 0.780, 3.68, and 0.791 respectively. The GST approach performed the worst in terms of spectral improvement as indicated *CC*, *RMSE*, and *SSIM* values of 0.4, 5.512, and 0.389 respectively.

Another problem to be investigated is the computational load associated with each fusion algorithm. Table 5 shows the processing time in seconds during the fusion process. GST is the cheapest classifier with 0.86 seconds/km^2. This is because the GST fusion algorithm adopts simpler computations as compared with the wavelet and hybrid approaches. Wavelet ranked the second with 1.22 second/km^2. Hybrid, on the other hand, is the most complex fusion algorithm with 1.31 second/km^2. However, it is still comparable with wavelet.

4.4 Classification Accuracy

The spectral reflectance characteristics of the pansharpened images have also been compared. Training samples describing the spectral signature for four LULC classes in each pan-sharpened image have been collected. In this regard, polygons of almost the same size have been manually digitized for buildings, roads, trees, and cultivated fields. As a result, three diagrams representing the DNs of classes have been generated for the red band, one diagram for each pansharpening approach as shown in Figure 7a, b and c. The GST pansharpened image may result in deteriorated classification results since trees are not represented in the diagram and cultivated fields are partially overlapped with class roads as shown in Figure 7a. For the wavelet fused image, a high degree of spectral similarities between trees and roads can be observed. Trees are completely overlapped with roads as shown in Figure 7b. On the other hand, the clear separation for DN values obtained for the hybrid fusion approach, Figure 7c indicates completely distinct training samples, which is essential for better classification. This analysis indicates the effectiveness of the proposed hybrid approach no matter in the spectral or spatial domain.

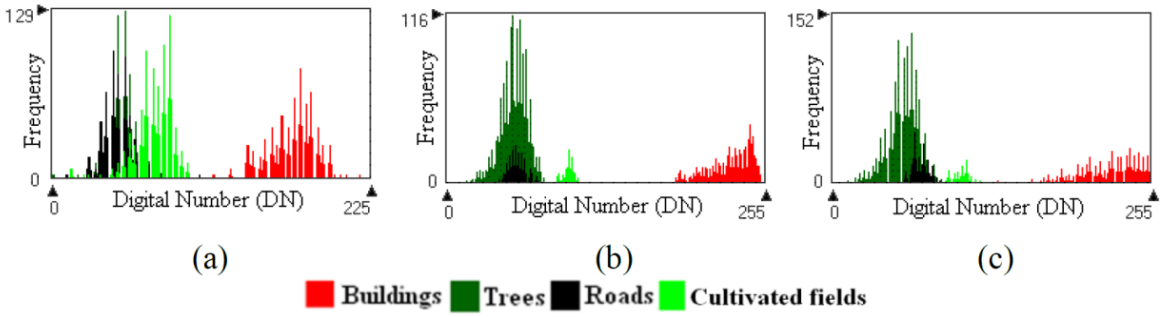

Figure 7: Spectral signatures of four training samples based on the red band: (a) GST; (b) wavelet; (c) hybrid approaches

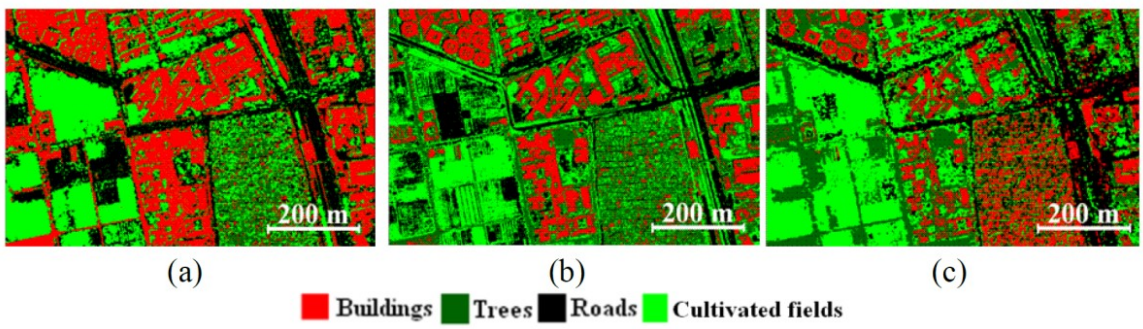

Figure 8: Classifications using the pansharpened images. (a) GST; (b) Wavelet; (c) Hybrid approaches

Table 6: *OA*, *PA*, and *UA* of the classification results obtained for the hybrid, GST, and wavelet fused images. Bold values indicate the best and underlined values indicate the worst

Method	***Overall Accuracy (%)***	***Class Accuracy (%)***							
		Buildings		***Trees***		***Roads***		***Grass***	
		PA	***UA***	***PA***	***UA***	***PA***	***UA***	***PA***	***UA***
GST	<u>37.60</u>	<u>41.88</u>	99.98	**82.68**	32.57	<u>20.67</u>	**99.45**	<u>0.00</u>	<u>0.00</u>
Wavelet	60.25	67.98	<u>99.55</u>	71.17	<u>24.59</u>	49.43	78.80	**99.13**	**38.52**
Hybrid	**66.67**	**73.82**	**100.00**	<u>31.25</u>	**33.72**	**71.70**	<u>74.31</u>	75.94	6.08

To assess the effectiveness of the proposed hybrid method, the pansharpened images have been used as inputs for the maximum likelihood classifier. To meet the objective, the overall accuracy *OA* has been assessed to validate the classification results for the three tested approaches as presented in Table 6. The results indicate that the obtained images by the proposed hybrid method have resulted in the best classification accuracy with 66.67% *OA*, followed by the wavelet fused image with 60.25% *OA*. The GST fused image produced the worst classification result with an OA of 37.60%. The relatively low *OA* indicates that the GST fused images are unsatisfactory for classification purposes. On the other hand, most of the PA and UA values have also been improved, in most cases, when the hybrid-based fused image was applied as inputs for the maximum likelihood classifier.

This investigation suggests that the hybrid fusion algorithm takes advantage of GST and wavelet fusion algorithms to achieve high quality pansharpened images. It is worth mentioning that, no single fusion algorithm has performed the best for all individual classes. A typical example is that the hybrid fusion results performed the worst for classification of trees with *PA* of 31.25%, and roads with *UA* of 31.25%. On the other hand, it outperformed the GST and wavelet for remaining classes. Thus, users should select the fusion algorithm that performs the best for a specific class. In term of applicability in real automatic analyzed image project in very massive materials, parallel processing units are needed since hybrid fusion requires relatively high computational complexities (Figure 8).

5. Conclusion

This study proposed a FMV-based approach for combining PAN archival aerial photographs with MS IKONOS imagery. Extensive experiments indicated that the proposed approach performed the best in terms of spatial improvement and spectral preservation. In terms of spatial consistency, the average *HCC* values obtained for the GST and hybrid fusions are above 0.8 indicating strong correlations between the obtained images and the original high-resolution one. The wavelet fusion showed a lower *HCC* value of around 0.4. In terms of spectral information, the GST fusion resulted in spectral distortions with a blurry fused image. The wavelet fusion shows better spectral preservation than the GST approach. However, this comes at the expense of spatial enhancement. The hybrid fusion performed the best with higher *CC*, *UIQI*, and *SSIM* values, 0.967, 0.96, and 0.956 respectively, as well as lower *RMSE* and *DIV* values of 1.51 and 1.68 respectively. Also, the processing time of the proposed fusion approach is slightly higher than the GST and wavelet approaches. This is because more sophisticated calculations have been involved for improved fusion results. On the other hand, the hybrid fusion has proved to be effective for LULC classification with 66.67% *OA* followed by the wavelet fusion with 60.25% *OA*. The GST fusion performed the worst with *an OA* of 37.60%. On the other hand, most of the class accuracies have also been improved with clear separation for DN values. As future work, more pansharpening algorithms have to be added to the hybrid system based on FMV in order to take advantage from their complementary characteristics. As well, the impact of image super-resolution on image pansharpening has to be investigated to yield better-fused images.

Acknowledgments

The author acknowledges Giza Utility Data Centre (GUDC)/Egypt for providing the MS IKONOS image and the Egyptian Survey Authority (ESA) for providing the PAN aerial images. The author is also indebted to anonymous reviewers for helpful comments which improved the manuscript.

References

Aiazzi, B., Baronti, S. and Selva, M., 2007, Improving Component Substitution Pansharpening Through Multivariate Regression of MS + Pan Data. *IEEE Transactions on Geoscience and Remote Sensing*, Vol. 45(10), 3230-3239. doi.org/10.1109/TGRS.2007.901007.

Azarang, A. and Ghassemian, H., 2017, A New Pansharpening Method using Multiresolution Analysis Framework and Deep Neural Networks. *2017 3rd International Conference on Pattern Recognition and Image Analysis (IPRIA)*, 19-20 April 2017, Shahrekord, Iran, 1-6. doi.org/10.1109/PRIA.2017.7983017.

Burt, P. and Adelson, E., 1983, The Laplacian Pyramid as a Compact Image Code. *IEEE Transactions on Communications*, Vol. 31(4), 532-540. doi.org/10.1109/TCOM.1983.1095851.

Carper, W., Littlesand, T. and Kiefer, R., 1990, The Use of Intensity-Hue-Saturation Transformations for Merging SPOT Panchromatic and Multispectral Image Data. *Photogrammetric Engineering and Remote Sensing*, Vol. 56(4), 459–467.

Congalton, R. G., 1991, A Review of Assessing the Accuracy of Classifications of Remotely Sensed Data. *Remote Sensing of Environ*ment, Vol. 37(1), 35-46. doi.org/10.1016/00344257(91)90-048-B.

Coltuc, D., Bolon, P. and Chassery, J. M., 2006, Exact Histogram Specification, *IEEE Transactions on Image Processing*, Vol. 15(5), 1143 – 1152. doi.org/10.1109/TIP.2005.864170.

Do, M. N. and Vetterli, M., 2005, The Contourlet Transform: An Efficient Directional Multiresolution Image Representation. *IEEE Transactions on Image Processing*, Vol. 14(12), 2091–2106. doi.org/10.1109/TIP.2005.859376.

Duran, J., Buades, A., Coll, B., Sbert, C. and Blanchet, G., 2017, A Survey of Pansharpening Methods with a New Band-Decoupled Variational Model. *ISPRS Journal of Photogrammetry and Remote Sensing*, Vol. 125(2017), 78-105. doi.org/10.1016/j.isprsjprs.-2016.12.013.

Ehlers, M., Klonus, S., Astrand, P. and Rosso, P., 2010, Multisensor Image Fusion for Pansharpening in Remote Sensing. *International Journal of Image and Data Fusion*, Vol. 1(1), 25-45. doi.org/10.1080/19479830903561985.

Ewiak, I., Siok, K. and Jenerowicz, A., 2016, Functionality Assessment of Algorithms for the Coloring of Images in Terms of Increasing Radiometric Values of Aerial Photographs Archives, *Arch Fotogram Kartogr Teledetekcji*, Vol. 28 (2016), 11–24. doi.org/10.14681-/afkit.2016.001.

Ewiak, I., Siok, K., Schismak, A. and Jenerowicz, A., 2018, Improvement of Interpretability of Archival Aerial Photographs using Remote Sensing Tools. *Proceedings of the SPIE, 10789,*

10-13 September 2018, Berlin, Niemcy, 8 (on CD-ROM). doi.org/10.1117/12.2325813.

Faragallah, O. S., 2018, Enhancing Multispectral Imagery Spatial Resolution using Optimized Adaptive PCA and High-Pass Modulation. *International Journal of Remote Sensing*, Vol. 39(20), 6572-6586. doi.org/10.1080/01431161.-2018.1463112.

Gong, Y., Lim, T. J. and Farhang–Boroujeny, B., 2001, Adaptive Least Mean Square CDMA Detection with Gram–Schmidt Pre–processing. *IEE Proceedings: Communications*, Vol. 148(4), 249-254. DOI: 10.1049/ip-com:20010274.

He, Z., Li, J., Liu, K., Liu, L. and Tao, H., 2018, Kernel Low-Rank Multitask Learning in Variational Mode Decomposition Domain for Multi-/Hyperspectral Classification. *IEEE Transactions on Geoscience and Remote Sensing*, Vol. 56(7), 4193-4208. doi.org/10.1109/TGRS.2018.2828612.

Herrera, F. and Verdegay, J. L., 1996, A Linguistic Decision Process in Group Decision Making. *Group Decision and Negotiation*, Vol. 5(1996), 165-176. doi.org/10.1007/BF00419908.

Hu, J., He, Z. and Wu, J., 2019, Deep Self-Learning Network for Adaptive Pansharpening. *Remote Sensing*, Vol. 11(20), 2395. doi.org/10.3390-/rs11202395.

Javan, F., Samadzadegan, F., Mehravar, S., Toosi, A., Khatami, R. and Stein, A., 2021, A Review of Image Fusion Techniques for Pan-Sharpening of High-Resolution Satellite Imagery. *ISPRS Journal of Photogrammetry and Remote Sensing*, Vol. 171(2021), 101-117. doi.org/10.-1016/j.isprsjprs.2020.11.001.

Jenerowicz, A., Kaczynski, R., Siok, K. and Schismak, A., 2018b, Data Fusion for High Accuracy Classification of Urban Areas. *Proceedings of SPIE 10793, Remote Sensing Technologies and Applications in Urban Environments III,* 1079315, 9 October 2018, Berlin, Germany, 15 (on CD-ROM). doi.org/10.1117/12.2325809.

Jenerowicz, A., Siok, K., Woroszkiewicz, M. and Orych, A., 2018a, The Fusion of Satellite and UAV Data: Simulation of High Spatial Resolution Band, *Proceedings of the Remote Sensing for Agriculture, Ecosystems, and Hydrology,* 11-14 September 2017, Warsaw, Poland, 12 (on CD-ROM). doi.org/10.11-17/12.2278669.

Jiang, D., Zhuang, D. and Huang, Y., 2013, Investigation of image fusion for remote sensing application, Chapter 1 in *New Advances in Image Fusion* (Ed. M. Qiguang). IntechOpen, London, UK. doi.org/10.5772/56946.

Johnson, B. A., Tateishi, R. and Hoan, N. T., 2013, A Hybrid Pansharpening Approach and Multiscale Object-Based Image Analysis for Mapping Diseased Pine and Oak Trees. *International Journal of Remote S*ensing, Vol. 34(20), 6969-6982. doi.org/10.1080/014311-61.2013.810825.

Kahramana, S. and Ertürk, A., 2017, A Comprehensive Review of Pansharpening Algorithms Göktürk-2 Satellite Images. *ISPRS Annals of the Photogrammetry, Remote Sensing and Spatial Information Sciences*, 4(4W4), 263-270. doi.org/10.5194/isprs-annals-IV-4-W4-263-2017.

Kaimaris, D., Patias, P., Mallinis, G. and Georgiadis, C., 2020, Data Fusion of Scanned Black and White Aerial Photographs with Multispectral Satellite Images. *Sci*., Vol. 2(2), 1-13. doi.org/-10.3390/sci1020036.

Klonus, S., 2008, Comparison of Pansharpening Algorithms for Combining Radar and Multispectral Data. *International Archives of the Photogrammetry, Remote Sensing and Spatial Information Sciences*, 3-11 July, Beijing, China, 189-194.

Krizhevsky, A., Sutskever, I. and Hinton, G.E., 2012, Imagenet Classification with Deep Convolutional Neural Networks. *Advances in Neural Information Processing Systems*, Vol. 25(2), 1097-1105. doi.org/10.1145/3065386.

Laben, C. A., Bernard, V. and Brower, W., 2000, Process for Enhancing the Spatial Resolution of Multispectral Imagery using Pan-Sharpening. United States Patent Application No. 6,011,875. https://patents.google.com/patent/US6011875A/en. Accessed 8 March 2021.

Lemeshewsky, G. P., 2002, Multispectral Image Sharpening using a Shift-Invariant Wavelet Transform and Adaptive Processing of Multiresolution Edges. *Proceedings of the Visual Information Processing XI; International Society for Optics and Photonics*, 30 July 2002, Orlando, FL, United States, 189-200. doi.org/10.1117-/12.477580.

Li, Z., Jing, Z. and Yang, X., 2005, Color Transfer Based Remote Sensing Image Fusion using Non-Separable Wavelet Frame Transform. *Pattern Recognition Letters*, Vol. 26(13), 2006-2014. doi.org/10.1016/j.patrec.2005.02.010.

Liao, W., Huang, X., Coillie, F. V., Gautama, S., Pizurica, A., Philips, W., Liu, H., Zhu, T., Shimoni, M., Moser, G. and Tuia, D., 2015, Processing of Multiresolution Thermal

Hyperspectral and Digital Color Data: Outcome of the 2014 IEEE GRSS Data Fusion Contest. *IEEE Journal of Selected Topics in Applied Earth Observations and Remote Sensing*, Vol. 8(6), 2984-2996. doi.org/10.1109/JSTARS.201-5.2420582.

Li, X., Zhang, Y., Gao, Y. and Yue, S., 2016, Using Guided Filtering to Improve Gram-Schmidt Based Pansharpening Method for GeoEye-1 Satellite Images. *4th International Conference on Information Systems and Computing Technology (ISCT 2016) Advances in Computer Science Research*, Vol. 64, 33-37.

Liu, Z., Li, G., Mercier, G., He, Y. and Pan, Q., 2016, Change Detection in Heterogenous Remote Sensing Images via Homogeneous Pixel Transformation. *IEEE Transactions on Image Processing*, Vol. 27(4), 1822-1834. doi.org/10.1-109/TIP.2017.2784560.

Maglione, P., Parente, C., Vallario, A., 2016, Pan-Sharpening Worldview-2: IHS, Brovey and Zhang Methods in Comparison. *International Journal of Engineering, Science and Technology*, Vol. 8(2), 673–679.

Matteoli, S., Diani, M. and Corsini, G., 2018, Automatic Target Recognition within Anomalous Regions of Interest in Hyperspectral Images. *IEEE Journal of Selected Topics in Applied Earth Observations and Remote Sensing*, Vol. 11(4), 1056-1069. doi.org/10-.1109/JSTARS.2018.2810336.

Mhangara, P., Mapurisa, W. and Mudau, N., 2020, Comparison of Image Fusion Techniques using Satellite Pour l'Observation De La Terre (SPOT) 6 Satellite Imagery. *Applied Sciences*, Vol. 10(5), 1-13, doi.org/10.3390/app10051881.

Murray, N. J., Keith, D. A., Simpson, D., Wilshire, J. H. and Lucas, R. M., 2018, REMAP: An Online Remote Sensing Application for Land Cover Classification and Monitoring. *Methods in Ecology and Evol*ution, Vol. 9(2018), 2019-2027. doi.org/10.1111/2041-210X.13043.

O'Connell, M. J., 1974, Multivariate Least Squares Fitting Program using Modified Gream–Schmidth Transformations. *North–Holland Publishing Co.*, Vol. 8, 56–69. doi: 10.17632/cj-vg9bfs5t.1.

Pohl, C., 2016, Multisensor Image Fusion Guidelines in Remote Sensing. *IOP Conference Series: Earth and Environmental Science,* Vol. 34. doi.org/10.1088/1755-1315/34/1/012026.

Pouran, B., 2005, Comparison between Four Methods for Data Fusion of ETM+ Multispectral and Pan Images. *Geo-Spatial Information Sci*ence, Vol. 8(2005), 112–122. doi.org/10.100-7/BF02826847.

Pradhan, P. S., King, R. L., Younan, N. H. and Holcomb, D. W., 2006, Estimation of The Number of Decomposition Levels for a Wavelet-Based Multiresolution Multisensor Image Fusion. *IEEE Transactions on Geoscience and Remote Sensing*, Vol. 44(12), 3674-3686. doi.org/10.1109/TGRS.2006.881758.

Qu, Y., Qi, H. and Kwan, C., 2018, Unsupervised Sparse Dirichlet-Net for Hyperspectral Image Super-Resolution. *Proceedings of the IEEE Conference on Computer Vision and Pattern Recognition*, Lake City, UT, USA, 18–22 June 2018, 2511–2520.

Saheb, B., Subbarao, K. and Phani Kumar, S., 2013, A Survey on Voting Algorithms Used in Safety Critical Systems. *International Journal of Engineering and Computer Sci*ence, Vol. 2(7), 2272–2275.

Shahdoosti, H. R. and Ghassemian, H., 2016, Combining the Spectral PCA and Spatial PCA Fusion Methods by an Optimal Filter. *Information Fusion*, Vol. 27(2016), 150–160. doi.org/10.1016/j.inffus.2015.06.006.

Shocher, A., Cohen, N. and Irani, M., 2018, Zero-Shot Super-Resolution using Deep Internal Learning. *Proceedings of the IEEE Conference on Computer Vision and Pattern Recognition*, Lake City, UT, USA, 18–22 June 2018, 3118–3126.

Siok, K. and Ewiak, I., 2020, The Simulation Approach to the Interpretation of Archival Aerial Photographs. *Open Geosciences*, Vol. 12(1),1–10. doi.org/10.1515/geo-2020-0001.

Siok, K., Ewiak, I. and Jenerowicz, A., 2020, Multi-Sensor Fusion: A Simulation Approach to Pansharpening Aerial and Satellite Images. *Sensors*, Vol. 20(24), 1-18, doi.org/10.3390/-s20247100.

Siok, K., Jenerowicz, A. and Woroszkiewicz, M., 2017, Enhancement of Spectral Quality of Archival Aerial Photographs using Satellite Imagery for Detection of Land Cover. *Journal of Applied Remote Sens*ing, Vol. 11(3), 36001. doi.org/10.1117/1.JRS.11.036001.

Vaiopoulos, A. D. and Karantzalos, K., 2016, Pansharpening on the Narrow VNIR and SWIR Spectral Bands of Sentinel-2, *International Archives of the Photogrammetry, Remote Sensing and Spatial Information Sciences*, XLI-B7: 723–730. doi.org/10.5194/isprs-archives-XLI-B7-723-2016.

Vivone, G., Alparone, L., Chanussot, J., Mura, M.D., Garzelli, A., Licciardi, G., Restaino, R.

and Wald, L., 2015, A Critical Comparison Among Pansharpening Algorithms. *IEEE Transactions on Geoscience and Remote Sensing*, Vol. 53(5), 2565 – 2586. doi.org/10.1-109/TGRS.2014.2361734.

Wang, Z., Bovik, A. C., Sheikh, H. R. and Simoncelli, E. P., 2004, Image Quality Assessment: From Error Visibility to Structural Similarity. *IEEE Transactions on Image Process*ing, Vol. 13(4), 600–612. doi.org/10.11-09/TIP.2003.819861.

Wang, Z., Ziou, D., Armenakis, C., Li, D. and Li, Q., 2005, A Comparative Analysis of Image Fusion Methods. *IEEE Transactions on Geoscience and Remote Sensing,* Vol. 43(6), 1391-1402.

Xu, H., Ma, J., Shao, Z., Zhang, H., Jiang, J. and Guo, X., 2020, SDPNet: A Deep Network for Pan-Sharpening with Enhanced Information Representation. *IEEE Transactions on Geoscience and Remote Sensing*, Vol. 59(5), 4120–4134. doi.org/10.1109/TGRS.2020.3022-482.

Xu, Q., Zhang, Y. and Li, B., 2014, Recent Advances in Pansharpening and Key Problems in Applications. *International Journal of Image and Data Fusion*, Vol. 5(3), 175–195. doi.org/10.1-080/19479832.2014.889227.

Yager, R. R., 1998, On Ordered Weighted Averaging Aggregation Operators in Multicriteria Decision Making, *IEEE Transactions on Systems, Man, and Cybernetics: Systems*, Vol. 18(1), 183-190. doi.org/10.110-9/21.87068.

Zhang, K., Zhang, F. and Yang, S., 2019, Fusion of Multispectral and Panchromatic Images via Spatial Weighted Neighbor Embedding. *Remote Sensing*, Vol. 11(5), 557. doi.org/10.3390/rs1-1050557.

Zhang, Y., 2002, Automatic Image Fusion: A New Sharpening Technique for IKONOS Multispectral Images. *GIM International*, Vol. 16 (5), 54–57.

Zhang, Y., De Backer, S. and Scheunders, P., 2009, Noise-Resistant Wavelet-Based Bayesian Fusion of Multispectral and Hyperspectral Images. *IEEE Transactions on Geoscience and Remote Sensing*, Vol. 47(11), 3834–3843. doi.org/10.1109/TGRS.2009.2017737.

Zhong, S., Zhang, Y., Chen, Y. and Wu, D., 2017, Combining Component Substitution and Multiresolution Analysis: A Novel Generalized BDSD Pansharpening Algorithm. *IEEE Journal of Selected Topics in Applied Earth Observations and Remote Sensing*, Vol. 10(6), 2867–2875. doi.org/10.1109/JSTARS.2017.2697445.

Zhou, J., Civco, D. L. and Silander, J. A., 1998, A Wavelet Transform Method to Merge Landsat TM and SPOT Panchromatic Data. *International Journal of Remote Sensing*, Vol. 19 (4), 743–757. doi.org/10.1080/014311698215973.